applied sciences

MDPI

Article

CO_2 Sorption and Regeneration Properties of K_2CO_3/Al_2O_3-Based Sorbent at High Pressure and Moderate Temperature

Do-Yeong Ryu [1,2,†], Seongbin Jo [3,†], Tae-Young Kim [1], Soo-Yeong In [1], Jin-Hyeok Woo [1], Jong-Heon Lee [1], Ho-Jin Chae [1], Jae-Kuk Kim [2], Jae-Eun Hwang [2], Jae-Chang Kim [1,*] and Soo-Chool Lee [4,*]

1 Department of Chemical Engineering, Kyungpook National University, Daegu 41566, Korea; dyryu@jnk.or.kr (D.-Y.R.); tyoung0218@knu.ac.kr (T.-Y.K.); soo0@knu.ac.kr (S.-Y.I.); wjh8865@knu.ac.kr (J.-H.W.); rnswma123@knu.ac.kr (J.-H.L.); hwman777@knu.ac.kr (H.-J.C.)
2 JnK Co., Ltd., Daegu 41566, Korea; jkkim@jnk.or.kr (J.-K.K.); jehwang@jnk.or.kr (J.-E.H.)
3 Department of Chemical and Environmental Engineering, University of California-Riverside, Riverside, CA 92521, USA; sjo016@ucr.edu
4 Research Institute of Advanced Energy Technology, Kyungpook National University, Daegu 41566, Korea
* Correspondence: kjchang@knu.ac.kr (J.-C.K.); soochool@knu.ac.kr (S.-C.L.)
† These authors contributed equally to this work.

Abstract: In this study, the CO_2 sorption mechanisms and regeneration properties of alumina-based sorbent using K_2CO_3 loading under high-pressure and moderate temperature conditions were examined. To investigate the mechanism of CO_2 sorption, a zirconium-based sorbent was compared with an alumina-based sorbent. The CO_2 capture capacities of the PAI10, 20, 30, and 40 were 32.3, 63.0, 95.4, and 124.5 mg CO_2/g sorbent, respectively. To investigate the CO_2 sorption mechanism of an alumina-based sorbent, we performed XRD, TG/DTG, and FTIR analyses after CO_2 sorption in the presence of 10 vol% CO_2 and H_2O each at 200 °C and 20 atm. For PAI10–40 sorbents, $KHCO_3$ and $KAl(CO_3)(OH)_2$ phases were observed by TG/DTG and FTIR analysis. For PAI-*x* sorbents, it was confirmed that the captured CO_2 is desorbed completely at a temperature below 400 °C at 20 atm.

Keywords: CCUS; coal-fired power plant; pre-combustion; γ-Al_2O_3; $KHCO_3$; $KAl(CO_3)(OH)_2$

Citation: Ryu, D.-Y.; Jo, S.; Kim, T.-Y.; In, S.-Y.; Woo, J.-H.; Lee, J.-H.; Chae, H.-J.; Kim, J.-K.; Hwang, J.-E.; Kim, J.-C.; et al. CO_2 Sorption and Regeneration Properties of K_2CO_3/Al_2O_3-Based Sorbent at High Pressure and Moderate Temperature. *Appl. Sci.* **2022**, *12*, 2989. https://doi.org/10.3390/app12062989

Academic Editors: Kun Sang Lee, Jinhyung Cho and Jihoon Wang

Received: 14 February 2022
Accepted: 13 March 2022
Published: 15 March 2022

1. Introduction

Fossil fuels, coal, petroleum, and natural gas account for about 86 percent of the world's primary energy. Greenhouse gas emissions are associated with human activities [1]; in particular, carbon dioxide (CO_2) is a major greenhouse gas emitted into the atmosphere by coal-fired power plants. Improved power generation technology can help prevent global warming and climate change by reducing carbon dioxide emissions from coal-fired power plants. Currently, several technological processes for CO_2 capture have been widely investigated: pre-combustion, post-combustion, and oxyfuel technology. In the case of pre-combustion process, CO_2 capture occurs before combustion from the synthesis gas of an integrated gasification combined cycle (IGCC). The total pressure in the pre-combustion process is 20–70 atm, and the CO_2 content is between 15 and 60%. In addition, the separation of CO_2 is significantly easier because of the high CO_2 partial pressure when compared with the post-combustion process [2–4]. The capture of CO_2 using dry CO_2 sorbent is one of the most efficient techniques in an IGCC plant. The ideal dry solid CO_2 sorbent for applying the pre-combustion process must have a high CO_2 capture capacity, a fast sorption rate, high selectivity for carbon dioxide, a stable CO_2 capture capacity for multiple cycles, and excellent physical properties, due to the high pressure and moderate temperature [5,6]. Many researchers use inorganic materials such as magnesium oxide, aluminum oxide, hydrotalcite, calcium oxide, and lithium-containing material to develop a dry CO_2 sorbent, applicable in the pre-combustion process in IGCC plants [7–17]. K_2CO_3-promoted alumina-based CO_2 sorbents have several advantages over these materials, including a lower cost,

high physical strength, and a relatively high CO_2 capture capacity [18–30]. As a result, many researchers have been studying the interaction between carbon dioxide and alumina-based CO_2 sorbents loaded with K_2CO_3 at relatively low temperatures of below 150 °C and low atmospheric pressure.

To understand the interaction between CO_2 and K_2CO_3 loaded alumina-based CO_2 sorbent under high-pressure and moderate temperature conditions, we investigated the CO_2 capture capacity and sorption mechanism of a K_2CO_3 loading at 200 °C and 20 atm.

This article reports the CO_2 capture capacities and absorption mechanism of PAI10–40 sorbents prepared by the impregnation method. X-ray diffraction (XRD), thermogravimetric analysis/differential thermal gravimetry (TGA/DTG), and temperature-programmed desorption (TPD) experiments were also carried out to investigate the CO_2 sorption mechanism, physical change, and regeneration properties of an alumina-based sorbent, respectively after CO_2 sorption at 20 atm.

2. Materials and Methods

2.1. Preparation of the CO_2 Sorbent and Analysis

The aluminum oxide (Sigma Aldrich) and zirconium oxide (Sigma Aldrich) sorbent impregnated with K_2CO_3 (Sigma Aldrich) in this study was prepared by the impregnation method. The preparation procedure was as follows: Al_2O_3 and ZrO_2 supports were added to aqueous solutions of K_2CO_3 from 10 to 40 weight % in de-ionized water. Then, the solutions were mixed with a magnetic stirrer for 24 h at room temperature. After stirring, the mixed samples were dried in a vacuum rotary evaporator [5,19–22]. These samples were calcined in an air furnace for 5 h at 500 °C. The calcination temperature was raised to 500 °C at a rate of 5 °C/min and then ground and sieved to produce a particle size range of 150–250 μm in diameter. These CO_2 sorbents are denoted as PAI-*x* and PZI*x*, where P, A, Z, I, *x* represent potassium carbonate, aluminum oxide, zirconium oxide, the impregnation method, and the potassium carbonate loading amount, respectively.

The changes in the crystalline phase before and after CO_2 sorption were examined by XRD (Philips X'PERT) using Cu Kα radiation at the Korea Basic Science Institute. TGA and DTG (SDT Q600, TA instrument) were conducted to investigate the thermal characteristics after CO_2 sorption. Nitrogen gas was used as the carrier gas, and the CO_2 sorbent was heated from 30 °C to 500 °C at a ramping rate of 5 °C/min. The N_2 adsorption-desorption isotherms at −196 °C were recorded using a Micrometrics ASAP 2020 instrument to evaluate textural properties such as the BET surface area, pore volume, and pore size. The changes in the properties of the sorbents after CO_2 sorption were investigated by Fourier transform infrared (FTIR, PerkinElmer Inc., Waltham, MA, USA). The TPD experiment was conducted in a nitrogen atmosphere, and the sample was heated from 100 °C to 450 °C at a heating rate of 2 °C/min.

2.2. Apparatus and Procedure

The CO_2 capture capacity of the aluminum and zirconium oxide sorbents were conducted using a stainless steel fix-bed reactor with an outside diameter of 1 inch. The CO_2 sorbent was dried for 12 h at 350 °C in a nitrogen atmosphere to remove moisture and impurities from the sorbent surface. The CO_2 capture capacity of the CO_2 sorbent was investigated by packing 10 g of the sorbent into a stainless steel reactor and maintaining the CO_2 sorption pressure at 20 atm with a back pressure regulator. An analog pressure gauges and two digital pressure gauges were used to check pressures during CO_2 sorption. The composition of feed gases was 10 vol% CO_2, 10 vol% H_2O and the remainder was N_2. The GC column used in the analysis was a 1/8 inch stainless tube packed with Porapak Q. The outlet gas was automatically analyzed every 2 min with a thermal conductivity detector (Agilent, Santa Clara, CA, USA, 6890) equipped with an autosampler (Valco, Houston, TX, USA). The CO_2 capture capacity was calculated from the CO_2 breakthrough curve, which indicates the amount of CO_2 absorbed until the output concentration of CO_2 reaches 10 vol%, which is the same as the inlet concentration. The CO_2 capture capacity is

determined by the amount of CO_2 absorbed per 1 g of sorbent (mg CO_2/g sorbent). The CO_2 capture capacity was calculated according to Equation (1) as follows:

$$CO_2 \text{ capture capacity } = (\frac{P \times V_{CO_2}}{R \times T} \times M_{CO_2} \times t, \ milligram)/(grampersorbent) \quad (1)$$

3. Results

3.1. CO_2 Capture Capacity of a CO_2 Sorbent

Table 1 provides information on the surface area, pore volume, and pore size of ɣ-Al_2O_3, ZrO_2, PZI30 sorbent, and PAI-*x* sorbents. The bare ZrO_2 had a surface area of 8.05 m^2/g, a pore volume of 0.02 cm^3/g, and a pore size of 3.83 nm. The ɣ-Al_2O_3 had a surface area of 157.65 m^2/g, a pore volume of 0.31 cm^3/g, and a pore size of 4.91 nm. Compared with the ZrO_2 support material, the surface area and pore volume of the PZI30 sorbent decreased; it might be expected that the very low surface area and pore volume of PZI30 sorbent results in poor CO_2 capture capacity. When K_2CO_3 is loaded on the support materials, surface area decreases, whereas a significant change in pore size is not observed regardless of the K_2CO_3 loading amount. When the K_2CO_3 loading is 40 wt% (PAI40 sorbent), the surface area is reduced to about 17.3% compared with the Al_2O_3 support material, and the pore volume is also significantly reduced. The decrease in surface area and pore volume is caused by filling the pores or blocking the pore openings with K_2CO_3.

Table 1. Textural properties of ɣ-Al_2O_3, PZI30, and potassium-based alumina sorbents.

Sample	Surface Area (m^2/g)	Pore Volume (cm^3/g)	Pore Size (nm)
ɣ-Al_2O_3	157.65	0.31	4.91
ZrO_2	8.04	0.03	3.83
PZI30	3.92	0.02	3.82
PAI10	134.98	0.22	4.32
PAI20	69.67	0.17	4.32
PAI30	44.26	0.17	4.32
PAI40	27.37	0.09	4.31

Figure 1 presents the breakthrough curves (a) and the CO_2 capture capacity (b) per 1 g of sorbent for PAI10 to 40 and PZI30 sorbents in the presence of 10 vol% CO_2, 10 vol% H_2O, N_2 balance at 200 °C and 20 atm. Figure 1b shows the CO_2 capture capacities of PAI10 to 40 and PZI30 sorbents calculated from the CO_2 sorption breakthrough curves shown in Figure 1a. Under high-pressure conditions (20 atm), PZI30 sorbent was used to investigate the reaction mechanism of alumina-based sorbent. PZI30 and PAI10–40 sorbents had CO_2 capture capacities of 19.7 and 32.3, 63.0, 95.4, and 124.5 mg CO_2/g sorbent, respectively. CO_2 capture capacities of PAI-x sorbents increased with increasing K_2CO_3 loading. Compared with the PZI30 sorbent, the PAI30 sorbent showed a higher CO_2 capture capacity.

Figure 2 shows the amount of CO_2 sorption per 1 g K_2CO_3 as a function of the K_2CO_3 loading. The CO_2 sorption per 1 g K_2CO_3 was calculated from the CO_2 capture capacities of PZI30 and PAI10–40 sorbents, as shown in Figure 1. The CO_2 capture capacities of PAI10–40 sorbents were maintained at approximately 311.2–323.1 mg CO_2/g K_2CO_3. These calculated values corresponded to approximately 98–101% of the K_2CO_3 theoretical value of 318.4 mg CO_2/g K_2CO_3. However, the CO_2 capture capacity of PZI30 sorbent was approximately 65.7 mg CO_2/g K_2CO_3, which is equivalent to approximately 26% of the K_2CO_3 theoretical value. The differences in the CO_2 capture capacities of PZI30 and PAI10–40 sorbents mean that the CO_2 sorbents can be absorbed through different reaction mechanisms.

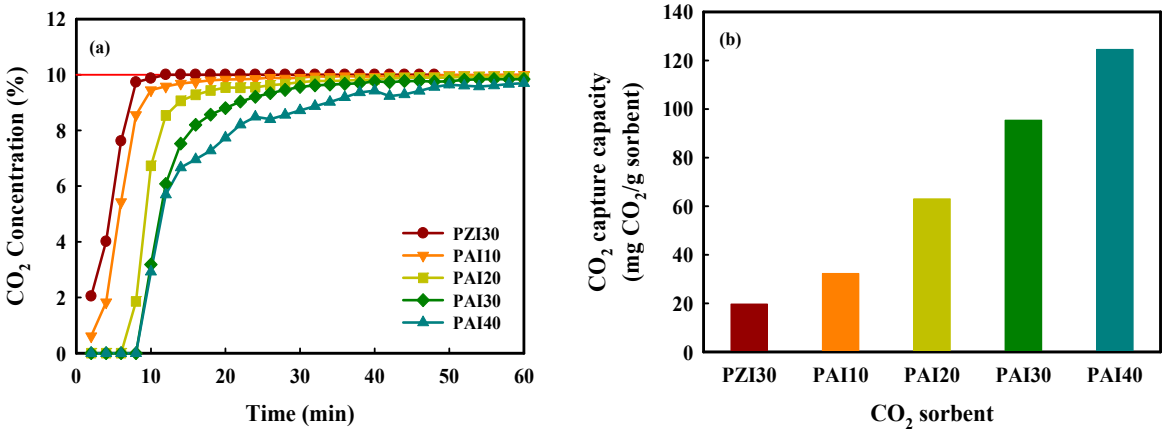

Figure 1. CO_2 breakthrough curves (**a**) and CO_2 capture capacities (**b**) of PZI30 and PAI10–40 sorbents according to K_2CO_3 loading at 20 atm.

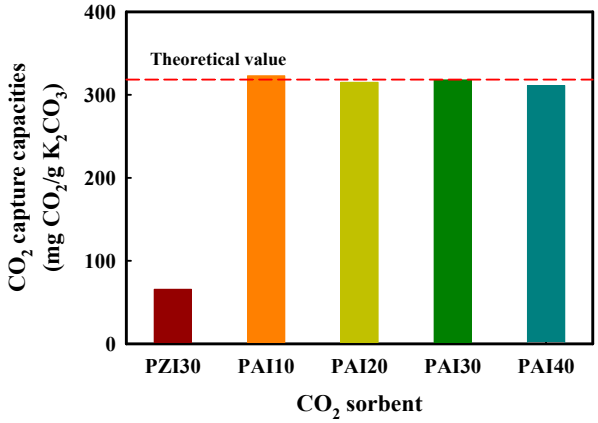

Figure 2. CO_2 capture capacities per 1 g of K_2CO_3 as a function of the amount of K_2CO_3 for PZI30 and PAI10–40 sorbents after CO_2 sorption in the presence of 10 vol% CO_2, 10 vol% H_2O, N_2 balance at 200 °C and 20 atm.

3.2. Physical Characteristic Analysis after CO_2 Sorption

The results of the XRD analysis of PZI30 and PAI10–40 sorbents conducted to identify the structural changes before and after CO_2 sorption are shown in Figure 3. The XRD patterns of PZI30 in the fresh state show the sharp peaks of ZrO_2 (JCPDS No. 83-0940) and small peaks of K_2CO_3 (JCPDS No. 16-0820). For PAI10–40 sorbents before CO_2 sorption, only K_2CO_3, and ɣ-Al_2O_3 (JCPDS No. 10-0425) phases were observed. In the case of PAI10–40 sorbents, the peak intensity of K_2CO_3 increased with increasing K_2CO_3 loading. For PZI30 sorbent, the $KHCO_3$ phase could not be detected after CO_2 sorption in the presence of water vapor at 200 °C and 20 atm, as shown in Figure 3II. After CO_2 sorption, on the other hand, the XRD patterns of PAI10–40 sorbents showed two phases: Al_2O_3, and $KAl(CO_3)(OH)_2$ (JCPDS No. 15-3303). XRD patterns of PAI10–40 sorbents showed no $KHCO_3$ phase after CO_2 sorption regardless of the K_2CO_3 loading. Based on the XRD results, the $KAl(CO_3)(OH)_2$ phase formed from K_2CO_3 and ɣ-Al_2O_3 over PAIx sorbents during CO_2 sorption in the presence of 10 vol% CO_2 and 10 vol% H_2O at 200 °C and 20 atm.

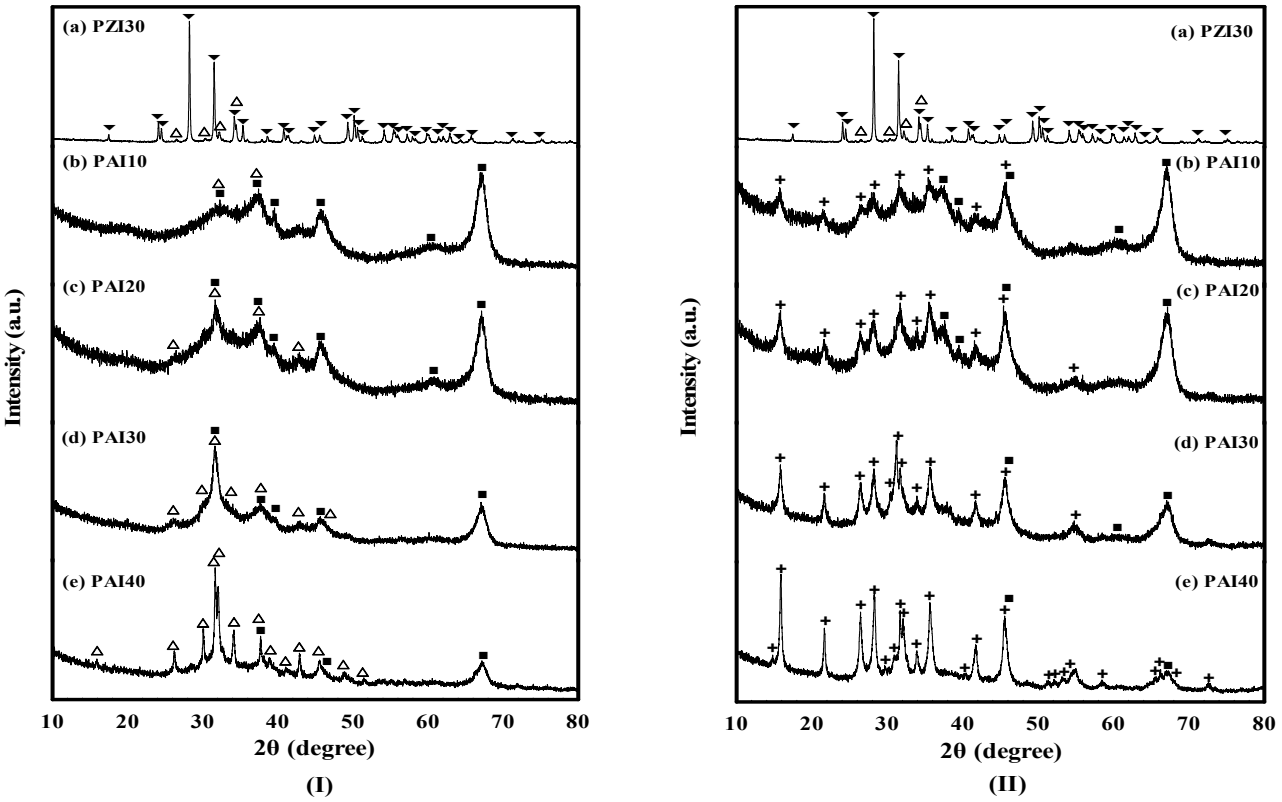

Figure 3. XRD patterns of the PZI30 and PAI10–40 sorbents before (**I**) and after (**II**) CO_2 sorption according to K_2CO_3 loading; (△) K_2CO_3, (▼) ZrO_2, (■) ɣ-Al_2O_3, (+) $KAl(CO_3)(OH)_2$.

FTIR analysis of PZI30, PAI10–40 sorbents, and pure $KHCO_3$ reagent (Sigma-Aldrich, CAS No. 298-14-6) was conducted to confirm the formation of the $KHCO_3$ structure after CO_2 sorption in the range of 400 to 4000 cm^{-1}. These results are shown in Figure 4. In all PZI30 and PAI10-40 sorbents, the broad peaks at a wavenumber of 3400 cm^{-1} (the expected bond is O-H) are attributed to H_2O on the surface. In the case of PAI-*x* and PZI30 sorbents after CO_2 sorption, the weak peaks at wavenumber 662 cm^{-1} (the expected bond is O_1CO_2), and 840 cm^{-1} (the expected bond is CO_3) are attributed to carbonate. In addition, the strong peaks at wavenumber 1007 cm^{-1} (the expected bond is C-O+C···O), 1402 cm^{-1} (the expected bond is O-H···O), and 1630 cm^{-1} (the expected bond is C=O) are attributed to bicarbonate species [17,24,27,31]. These results are in agreement with pure $KHCO_3$ analysis. The weak peaks at 1100 cm^{-1} of PAI10-40 sorbents are due to Al-O stretching and Al-O-H bending vibration, and the broad peaks at 1500 cm^{-1} of PAI10-40 sorbents are attributed to the H-O-H bend of absorbed H_2O [32]. The FTIR results show that for the K_2CO_3 loaded alumina-based CO_2 sorbent, the $KHCO_3$ structure was formed during CO_2 sorption in the presence of 10 vol% CO_2 and 10 vol% H_2O at 200 °C and 20 atm. We suggest that the $KHCO_3$ structure is formed during CO_2 sorption in the presence of water vapor at 200 °C and 20 atm [24–26]. According to the XRD and FTIR results, the alumina-based CO_2 sorbent could form the $KHCO_3$ phase and $KAl(CO_3)(OH)_2$ phase after CO_2 sorption in the presence of water vapor at high pressure and 200 °C.

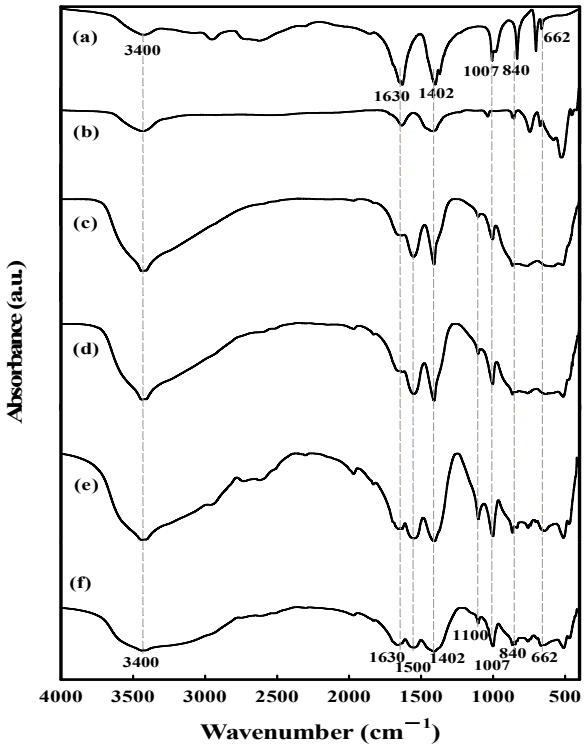

Figure 4. FTIR results of PZI30 and PAI10–40 sorbents after CO_2 sorption: (**a**) $KHCO_3$, (**b**) KZI30, (**c**) PAI10, (**d**) PAI20, (**e**) PAI30, (**f**) PAI40.

The results of TGA/DTG of PZI30 and PAI10–40 sorbents conducted to investigate the thermal properties after CO_2 sorption are shown in Figure 5. PZI30 and PAI10–40 sorbents showed weight loss at temperatures between 30 °C and 100 °C. This is due to the desorption of adsorbed water on the sorbent surface. The weight loss of PZI30 sorbent after CO_2 sorption at 20 atm was 5% at temperatures from 140 °C to 200 °C. The DTG peak of PZI30 sorbent showed one peak at the same temperature range as the weight loss range of TGA. Figure 3II shows that the PZI30 sorbent did not change structure after CO_2 sorption at 20 atm, but the TGA/DTG confirmed that the PZI30 sorbent showed weight loss at temperatures ranging from 140 °C to 200 °C, which is attributed to CO_2 desorption from the $KHCO_3$ phase. At temperatures ranging from 140 °C to 350 °C, the weight loss of the PAI10–40 sorbents was 5.73%, 7.28%, 10.63%, and 11.61%, respectively. The DTG peak of PAI10 and 20 sorbents showed one peak between 200 °C and 350 °C due to the decomposition of the $KAl(CO_3)(OH)_2$ structure. The DTG peak of PAI30 and 40 sorbents showed two peaks at 140 °C to 200 °C and 200 °C to 350 °C, respectively. In the case of 140 °C to 200 °C, it was confirmed that the temperature range of the DTG peak was the same as for the PZI30 sorbent. In the XRD analysis for PAI30 and 40 sorbents, no $KHCO_3$ structures were found after CO_2 sorption, but we confirmed a weight loss in the temperature range from 140 °C to 200 °C. The TGA/DTG results confirmed that for the PAI10–40 sorbents, there are two CO_2 sorption mechanisms involving $KHCO_3$ and $KAl(CO_3)(OH)_2$ structures formed with increasing K_2CO_3 loading under water vapor at high pressure [28].

From these analysis results, it was concluded that unlike for the PZI30 sorbent, the CO_2 absorption mechanism of the PAI-*x* sorbent was due to the formation of $KHCO_3$ and $KAl(CO_3)(OH)_2$ structures in the presence of water vapor in the conditions of 200 °C and 20 atm.

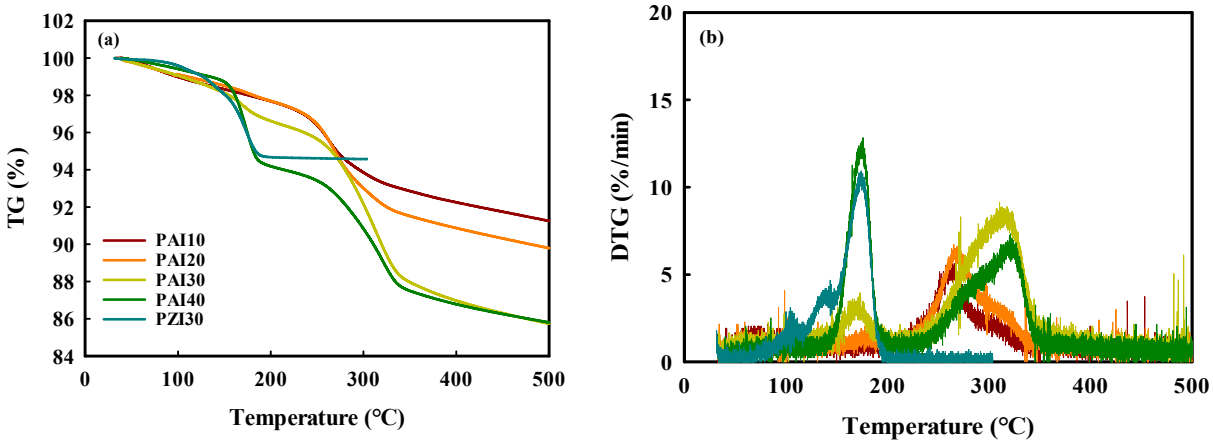

Figure 5. TG (**a**) and DTG (**b**) curves of PZI30 and PAI10–40 sorbents after CO_2 sorption according to K_2CO_3 loading.

3.3. TPD at 20 atm of PZI30 and PAI10–40 Sorbents

TPD experiments of PAI10–40 sorbents were conducted to examine the regeneration properties under 20 atm, as shown in Figure 6. In addition, a test of PZI30 sorbent was conducted to identify the decomposition temperature of the $KHCO_3$ structure at 20 atm. The CO_2 desorption of PAI-*x* sorbents started at 150 °C, and the desorbed CO_2 peak was observed in the temperature range from 150 °C to 400 °C. The TPD results of PAI10 and 20 sorbents showed one peak between 250 °C and 350 °C, and the TPD results of PAI30 and 40 sorbents showed two peaks between 150 °C and 400 °C. In the case of low K_2CO_3 loading such as PAI10 and 20, the CO_2 peak was produced by the decomposition of the $KAl(CO_3)(OH)_2$ structure. In the case of high K_2CO_3 loadings such as PAI30 and 40 sorbents, the CO_2 peak was produced by the decomposition of the $KHCO_3$ and $KAl(CO_3)(OH)_2$ structures. Particularly, the $KHCO_3$ decomposition of PAI30 and 40 sorbents appeared at the same temperature range as the PZI30 sorbent, and the CO_2 peak caused by the decomposition of $KAl(CO_3)(OH)_2$ increased with increasing K_2CO_3 loading. The CO_2 peak caused by $KHCO_3$ decomposition also increased due to increased K_2CO_3 loading. Based on the TPD results, the alumina-based CO_2 sorbent was confirmed to be capable of regeneration at temperatures below 400 °C at 20 atm. This study concluded that the potassium-loaded alumina-based sorbent had a higher CO_2 capture capacity than the zirconium-based sorbent due to the high surface area of alumina and the $KHCO_3$ and $KAl(CO_3)(OH)_2$ conversion. This means that these sorbents could be used as a support and additive to prepare a sorbent with the potential for CO_2 capture and regeneration under high and moderate temperature conditions.

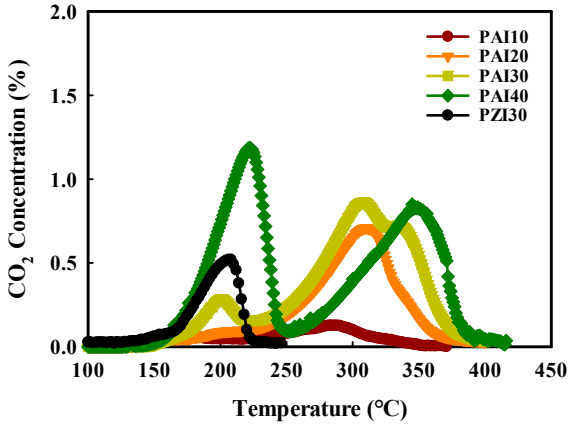

Figure 6. TPD results at 20 atm of PZI30 and PAI10–40 sorbents after CO_2 sorption at 20 atm.

4. Conclusions

This study examined the CO_2 absorption mechanisms and regeneration properties of alumina-based sorbents according to K_2CO_3 loading in the presence of 10 vol% CO_2, 10 vol% H_2O, N_2 balance at 200 °C and 20 atm. For the alumina-based sorbent loaded with K_2CO_3, such as PAI10–40, the CO_2 capture capacities were found to be 32.3, 63.0, 95.4, 124.5 mg CO_2/g sorbent, respectively, which was about 98% to 101% of the K_2CO_3 theoretical value. However, the CO_2 capture capacity of PZI30 sorbent was 19.7 mg CO_2/g sorbent, corresponding to 26% of the K_2CO_3 theoretical value. The higher CO_2 capture capacity of PAI-*x* sorbent relative to the PZI30 sorbent was confirmed by an XRD, FTIR analysis, and TPD experiment. This was attributed to $KHCO_3$ and $KAl(CO_3)(OH)_2$ structures. As for the regeneration properties measured in the TPD experiment, the PAI10 and 20 sorbents showed one peak due to the decomposition of $KAl(CO_3)(OH)_2$ at temperatures of 250 °C and 350 °C. The PAI30 and 40 sorbents showed two peaks due to the decomposition of $KHCO_3$ and $KAl(CO_3)(OH)_2$ at temperatures of 150 °C and 400 °C. In the case of PAI-*x* sorbent, the $KHCO_3$ structure generated during CO_2 sorption was confirmed to have the same decomposition temperature as the $KHCO_3$ structure generated after CO_2 sorption of PZI30 sorbent. This study demonstrated that the regeneration of an alumina-based sorbent is possible at temperatures lower than 400 °C. This low regeneration energy is advantageous because the CO_2 capture cost can be reduced under high pressure and moderate temperature conditions.

Author Contributions: Conceptualization, D.-Y.R., S.-C.L.; formal analysis, D.-Y.R., S.J., T.-Y.K.; investigation, J.-H.W., S.-Y.I., J.-H.L., H.-J.C., J.-K.K., J.-E.H.; supervision, S.-C.L., and J.-C.K.; writing—original draft, D.-Y.R., S.J.; writing—review and editing, S.J. and S.-C.L. All authors have read and agreed to the published version of the manuscript.

Funding: This work was supported by the Technology Innovation Program (No. 20015460) funded By the Ministry of Trade, Industry & Energy (MOTIE, Korea). This research was also supported by National R&D Program through the National Research Foundation of Korea (NRF) funded by Ministry of Science and ICT (No.2021M3I3A1084502).

Institutional Review Board Statement: Not applicable.

Informed Consent Statement: Not applicable.

Data Availability Statement: Not applicable.

Conflicts of Interest: The authors declare no conflict of interest.

References

1. Orr, F.M., Jr. CO_2 capture and storage: Are we ready? *Energy Environ. Sci.* **2009**, *2*, 449–458. [CrossRef]
2. Xiao, G.; Singh, R.; Chaffee, A.; Webley, P. Advanced adsorbents based on MgO and K_2CO_3 for capture of CO_2 at elevated temperatures. *Int. J. Greenhouse Gas Control.* **2011**, *5*, 634–639. [CrossRef]
3. Fisher, J.C.; Siriwardane, R.V.; Stevens, R.W., II. Process for CO_2 Capture from High-Pressure and Moderate-Temperature Gas Streams. *Ind. Eng. Chem. Res.* **2012**, *51*, 5273–5281. [CrossRef]
4. Siriwardane, R.V.; Stevens, R.W., Jr. Novel regenerable magnesium hydroxide sorbents for CO_2 capture at warm gas temperatures. *Ind. Eng. Chem. Res.* **2009**, *48*, 2135–2141. [CrossRef]
5. Lee, S.C.; Kwon, Y.M.; Chae, H.J.; Jung, S.Y.; Lee, J.B.; Ryu, C.K.; Yi, C.K.; Kim, J.C. Improving regeneration properties of potassium-based alumina sorbents for carbon dioxide capture from flue gas. *Fuel* **2013**, *104*, 882–885. [CrossRef]
6. Yong, Z.; Mata, V.; Rodrigues, A.E. Adsorption of carbon dioxide at high temperature—A review. *Sep. Purif. Technol.* **2002**, *26*, 195–205. [CrossRef]
7. Hwang, B.W.; Lim, J.H.; Chae, H.J.; Ryu, H.-J.; Lee, D.; Lee, J.B.; Kim, H.; Lee, S.C.; Kim, J.C. CO_2 capture and regeneration properties of MgO-based sorbents promoted with alkali metal nitrates at high pressure for the sorption enhanced water gas shift process. *Process Saf. Environ. Prot.* **2018**, *116*, 219–227. [CrossRef]
8. Wu, S.F.; Li, Q.H.; Kim, J.N.; Yi, K.B. Properties of a Nano CaO/Al_2O_3 CO_2 sorbent. *Ind. Eng. Chem. Res.* **2008**, *47*, 180–184. [CrossRef]
9. Ma, J.; Xu, Y.; Wu, Y.; Chen, X.; Cai, T.; Liu, D. Continuous CO_2 capture performance of K_2CO_3/Al_2O_3 sorbents in a novel integrated bubbling-transport fluidized reactor. *Ind. Eng. Chem. Res.* **2019**, *58*, 19733–19740. [CrossRef]

10. Koirala, R.; Gunugunuri, K.R.; Pratsinis, S.E.; Smirniotis, P.G. Effect of zirconia doping on the structure and stability of CaO-based sorbents for CO_2 capture during extended operating cycles. *J. Phys. Chem. C.* **2011**, *115*, 24804–24812. [CrossRef]
11. Mastin, J.; Aranda, A.; Meyer, J. New synthesis method for CaO-based synthetic sorbents with enhanced properties for high-temperature CO_2-capture. *Energy Procedia.* **2011**, *4*, 1184–1191. [CrossRef]
12. Zhou, Z.; Qi, Y.; Xie, M.; Cheng, Z.; Yuan, W. Synthesis of CaO-based sorbents through incorporation of alumina/aluminate and their CO_2 capture performance. *Chem. Eng. Sci.* **2012**, *74*, 172–180. [CrossRef]
13. Valverde, J.M. Ca-based synthetic materials with enhanced CO_2 capture efficiency. *J. Mater. Chem. A.* **2013**, *1*, 447–468. [CrossRef]
14. Tripoonsuk, C.; Maneewatthanakulphol, T.; Khantiudom, W.; Chalermsinsuwan, B.; Piumsomboon, P. Potassium Carbonate Supported on gamma-Alumina Sorbent Regeneration in Fluidized Bed Reactor for Carbon Dioxide Capture Technology. *Eng. J.* **2021**, *25*, 45–55. [CrossRef]
15. Choi, S.H.; Drese, J.H.; Jones, C.W. Adsorbent materials for carbon dioxide capture from large anthropogenic point sources. *ChemSusChem* **2009**, *2*, 796–854. [CrossRef] [PubMed]
16. Guo, L.; Wang, X.; Zhong, C.; Li, L. Synthesis and CO_2 capture property of high aspect-ratio Li_2ZrO_3 nanotubes arrays. *Appl. Surf. Sci.* **2011**, *257*, 8106–8109. [CrossRef]
17. Walspurger, S.; Cobden, P.D.; Haije, W.G.; Westerwaal, R.; Elzinga, G.D.; Safonova, O.V. In situ XRD detection of reversible dawsonite formation on alkali promoted alumina: A cheap sorbent for CO_2 capture. *Eur. J. Inorg. Chem.* **2010**, *2010*, 2461–2464. [CrossRef]
18. Zhao, C.; Chen, X.; Zhao, C.; Wu, Y.; Wu, D. K_2CO_3/Al_2O_3 for capturing CO_2 in flue gas from power plants. Part 3: CO_2 Capture Behaviors of K_2CO_3/Al_2O_3 in a Bubbling Fluidized-Bed Reactor. *Energy Fuels* **2012**, *26*, 3062–3068. [CrossRef]
19. Li, L.; Li, Y.; Wen, X.; Wang, F.; Zhao, N.; Xiao, F.; Wei, W.; Sun, Y. CO_2 capture over $K_2CO_3/MgO/Al_2O_3$ dry sorbent in a fluidized bed. *Energy Fuels* **2011**, *25*, 3835–3842. [CrossRef]
20. Lee, S.C.; Kwon, Y.M.; Ryu, C.Y.; Chae, H.J.; Ragupathy, D.; Jung, S.Y.; Lee, J.B.; Ryu, C.K.; Kim, J.C. Development of new alumina-modified sorbents for CO_2 sorption and regeneration at temperatures below 200 °C. *Fuel* **2011**, *90*, 1465–1470. [CrossRef]
21. Lee, S.C.; Cho, M.S.; Jung, S.Y.; Ryu, C.K.; Kim, J.C. Effects of alumina phases on CO_2 sorption and regeneration properties of potassium-based alumina sorbents. *Adsorption* **2014**, *20*, 331–339. [CrossRef]
22. Lee, S.C.; Kim, J.C. Dry potassium-based sorbents for CO_2 capture. *Catal. Surv. Asia.* **2007**, *11*, 171–185. [CrossRef]
23. Lee, S.C.; Choi, B.Y.; Lee, T.J.; Ryu, C.K.; Ahn, Y.S.; Kim, J.C. CO_2 absorption and regeneration of alkali metal-based solid sorbents. *Cat. Today* **2006**, *111*, 385–390. [CrossRef]
24. Lee, S.C.; Chae, H.J.; Lee, S.J.; Park, Y.H.; Ryu, C.K.; Yi, C.K.; Kim, J.C. Novel regenerable potassium-based dry sorbents for CO_2 capture at low temperatures. *J. Mol. Catal. B Enzym.* **2009**, *56*, 179–184. [CrossRef]
25. Lee, S.C.; Cho, M.S.; Kwon, Y.M.; Chae, H.J.; Jung, S.Y.; Ryu, C.K. Dhanusuraman Ragupathy, K.J.C. CO_2 sorption properties of nano-sized zirconia-based sorbents promoted with alkali metal carbonates. *J. Nanoelectron. Optoelectron.* **2012**, *7*, 460–465. [CrossRef]
26. Lee, S.C.; Kwon, Y.M.; Jung, S.Y.; Lee, J.B.; Ryu, C.K.; Kim, J.C. Excellent thermal stability of potassium-based sorbent using ZrO_2 for post combustion CO_2 capture. *Fuel* **2014**, *115*, 97–100. [CrossRef]
27. Nyquist, R.A.; Kagel, R.O. *The Handbook of Infrared and Raman Spectra of Inorganic Compounds and Organic Salts*; Academic Press: Cambridge, MA, USA, 1971.
28. Jo, S.B.; Lee, S.C.; Chae, H.J.; Cho, M.S.; Lee, J.B.; Baek, J.I.; Kim, J.C. Regenerable potassium-based alumina sorbents prepared by CO_2 thermal treatment for post-combustion carbon dioxide capture. *Korean J. Chem. Eng.* **2016**, *33*, 3207–3215. [CrossRef]
29. Ma, J.; Zhong, J.; Bao, X.; Chen, X.; Wu, Y.; Cai, T.; Liu, D.; Liang, C. Continuous CO_2 capture performance of K_2CO_3/Al_2O_3 sorbents in a novel two-stage integrated bubbling-transport fluidized reactor. *Chem. Eng. J.* **2021**, *404*, 126465. [CrossRef]
30. Amiri, M.; Shahhosseini, S. Optimization of CO_2 capture from simulated flue gas using K_2CO_3/Al_2O_3 in a Micro fluidized bed reactor. *Energy Fuels* **2018**, *32*, 7978–7990. [CrossRef]
31. Lucazeau, G.; Novak, A. Low temperature Raman spectra of $KHCO_3$ single crystal. *J. Raman Spectrosc.* **1973**, *1*, 573–586. [CrossRef]
32. Dembowski, M.; Loring, J.S.; Bowden, M.E.; Reynolds, J.G.; Graham, T.R.; Rosso, K.M.; Pearce, C.I. The controlling role of atmosphere in dawsonite versus gibbsite precipitation from tetrahedral aluminate species. *Dalton Trans.* **2021**, *50*, 13438–13446. [CrossRef] [PubMed]